BioChem Press

Inter*net* Electronic Journal of
Molecular Design

Editor: Ovidiu Ivanciuc

Special issue dedicated to Professor Haruo Hosoya on the occasion of the 65th birthday
Part 8

Guest Editor: Jun–ichi Aihara

Edge Configurations on a Regular Octahedron. Their Exhaustive Enumeration and Examination With Respect to Edge Numbers and Point–Group Symmetries

Shinsaku Fujita and Nobukazu Matsubara

Department of Chemistry and Materials Technology, Kyoto Institute of Technology, Matsugasaki, Sakyo–ku, Kyoto, 606–8585 Japan

Citation of the article:
  S. Fujita and N. Matsubara, Edge Configurations on a Regular Octahedron. Their Exhaustive Enumeration and Examination With Respect to Edge Numbers and Point–Group Symmetries, *Internet Electron. J. Mol. Des.* **2003**, *2*, 224–241, http://www.biochempress.com.

Edge Configurations on a Regular Octahedron. Their Exhaustive Enumeration and Examination With Respect to Edge Numbers and Point–Group Symmetries[#]

Shinsaku Fujita* and Nobukazu Matsubara

Department of Chemistry and Materials Technology, Kyoto Institute of Technology, Matsugasaki, Sakyo–ku, Kyoto, 606–8585 Japan

Abstract

Motivation. The versatility of the USCI (unit–subduced–cycle–index) approach is demonstrated in characterizing the symmetries of octahedral complexes.

Method. Edge configurations on a regular octahedron have been combinatorially enumerated by the PCI (partial–cycle–index) method, which is one of the four methods of the USCI approach.

Results. Thereby, the complete set of edge configurations has been obtained, where all edge configurations are classified by virtue of two criteria, *i.e*., the numbers of edges and the point–group symmetries. The latter criterion enables us to examine chiral and achiral edge configurations, where complementary configurations are discussed in terms of the subductions of coset representations.

Conclusions. The USCI approach provides a common tool to systematize inorganic stereochemistry as well as organic stereochemistry.

Keywords. Octahedral complex; edge configuration; chiral descriptor; group theory.

Abbreviations and notations	
CI, cycle index	SCI, subduced cycle index
OC–6, octahedron with 6 positions (polyhedral symbol)	CR, coset representation
USCI–CF, unit subduced cycle index with chirality fittingness	PCI, partial cycle index
	USCI, unit subduced cycle index

1 INTRODUCTION

Brorson *et al*. [1] reported exhaustive examination of edge configurations on a regular octahedron in order to analyze chirality descriptors of the Δ/Λ system for distinguishing enantiomers of octahedral complexes. They provided the complete set of octahedral edge configurations after removal of duplication by computer, where they gave the table of 144 edge configurations in an itemized manner with respect to the number of occupied edges. The set,

---

[#] Dedicated to Professor Haruo Hosoya on the occasion of the 65th birthday.
* Correspondence author; phone: 075–724–7537; fax: 075–724–7580; E–mail: fujitas@chem.kit.ac.jp.

however, was not itemized with respect to point–group symmetries, so that the order of listing configurations in the original table [1] was rather random from a symmetrical point of view. As a result, the point–group symmetrical nature of each configuration had to be examined one by one in additional procedures, as found in von Zelewsky's textbook (pp. 119–128 in Ref. [2]). Such additional one–by–one examination came from the neglect of recent developments in combinatorial enumerations, as implied in the words of von Zelewsky (p. 11 in Ref. [2]): "The formal description (of combinatorial enumerations) becomes so involved that it is, at least in actual cases, often not very practical to apply these methods. This book is written for the experimental chemist, and not for the mathematical chemist. The chemist who has to solve a stereochemical problem, such as finding the number of possible isomers of a molecule, will generally not go to the trouble of using abstruse mathematical methods." The latter attitude of the chemist unfortunately stems from his/her knowledge of mathematical methods of the first generation, *e.g.*, Pólya's theorem [3,4]. In such mathematical methods of the first generation [5,6], the itemization of isomers was concerned only with the number of objects (*e.g.*, occupied edges in the enumeration of edge configurations of octahedral complexes by Brorson *et al*. [1]), so that the chemist would expect little additional information, so long as he/she believed that almost equivalent results could be obtained by manual enumeration (or sometimes by computer) [7]. However, since more informative methods of the second and third generations have been developed during the last two decades, a well–balanced attitude is necessary for the chemist not to miss useful pieces of information.

Mathematical methods of the second generation for combinatorial enumeration took both molecular formulas (the number of objects) and symmetries into consideration [8–13]. Mark tables introduced by Burnside [14] or framework groups introduced by Pople [15] were combined with permutation groups in order to take account of isomer symmetries. Although these methods worked well as sophisticated tools of combinatorial enumerations, further devices were necessary to discuss stereochemical problems.

As a mathematical method of the third generation, we have developed the USCI (unit–subduced–cycle–index) approach, where we have pointed out the importance of coset representations (CR) $\mathbf{G}(/\mathbf{G}_i)$ [16]. On the basis of the chirality/achirality properties of the groups $\mathbf{G}$ and $\mathbf{G}_i$, we have proposed the concept of sphericity and have applied it to understanding and solving stereochemical problems, *e.g.*, the redefinition of prochirality [16,17], topicity [18,19], stereogenicity [19], and anisochrony [20]. Moreover, we have proposed the subduction of coset representations and unit subduced cycle indices (USCIs) as new concepts [21]. The concepts have been applied to combinatorial enumeration [21] as well as to understanding and solving stereochemical problems [22,23], *e.g.*, systematic classification of molecular symmetries [24] and systematic design of achiral and chiral molecules [25].

As clarified in the preceding paragraphs, the present article will be devoted to discuss edge

configurations of octahedral complexes by means of the USCI approach, where combinatorial enumerations and stereochemical investigations are combined intimately. Since our efforts have mainly focused on vertex configurations in investigating inorganic compounds [26,27], the present paper on edge configurations will provide a new prospect of the USCI approach. As a result, it will show that the chemist who has to solve a stereochemical problem can rely on informative mathematical methods based on the USCI approach.

2 DESYMMETRIZATION OF AN OCTAHEDRAL SKELETON

Stereochemistry of octahedral complexes is usually discussed by using an octahedral skeleton (I) (Figure 1), which is designated by the polyhedral symbol OC–6 [28]. The arrangements of polydentate ligands on OC–6 are abstractly represented by edge configurations, in which each occupied edge is marked with a thick line. Each edge configuration is derived by the placement of a set of thick edges on the twelve unoccupied (thin) edges of OC–6 (I). Since the OC–6 belongs to O_h–symmetry, such derivation can be regarded as desymmetrization into a subgroup of the O_h–symmetry.
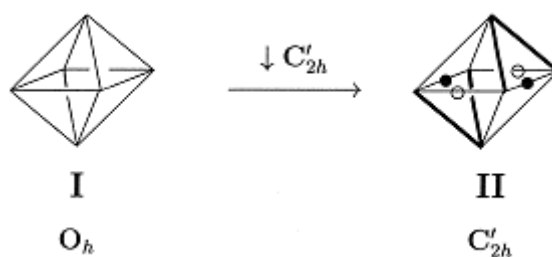

Figure 1. Derivation of C_{2h}'–configuration from an O_h–skeleton

The point group O_h has 33 subgroups up to conjugacy. They have been discussed in detail in terms of an irredundant set of subgroups [26]. When two or more subgroups belong to the same point group but not conjugate within the group O_h, they are differentiated by the addition of primes. For example, the point groups C_2 and C_2' represent chiral subgroups of order 2, where the group $C_2 = \{I, C_{2(3)}\}$ stems from the two–fold axis through the top and bottom vertices, while the group $C_2' = \{I, C_{2(1)}'\}$ is based on a two–fold axis bisecting a pair facing edges. Note that the symbol I represents an identity operation and that each number in the parentheses of $C_{2(3)}$ or $C_{2(1)}'$ is an ID number to differentiate conjugate operations from each other. The former two–fold axis corresponds to those of $C_{2v} = \{I, C_{2(3)}, \sigma_{h(2)}, \sigma_{h(3)}\}$, $C_{2v}' = \{I, C_{2(3)}, \sigma_{d(2)}, \sigma_{d(6)}\}$, $C_{2h} = \{I, C_{2(3)}, \sigma_{h(1)}, i\}$, while the latter one is relevant to $C_{2v}'' = \{I, C_{2(1)}', \sigma_{h(1)}, \sigma_{d(1)}\}$ and $C_{2h}' = \{I, C_{2(1)}', \sigma_{d(6)}, i\}$. The symbol σ_h with an ID number in parentheses represents a mirror plane containing four vertices (and four edges), while the symbol σ_d with an ID number in parentheses designates a mirror plane that contains two vertices and intersects two edges faced each other.

In the light of the USCI approach, the twelve edges are recognized to form a twelve–membered orbit (equivalence class), which is assigned to a coset representation (CR) represented by the symbol $\mathbf{O}_h(/\mathbf{C}_{2v}'')$. The symbol $\mathbf{O}_h(/\mathbf{C}_{2v}'')$ indicates that the global symmetry of the OC–6 (I) is $\mathbf{O}_h$ and the local symmetry of each vacant edge is $\mathbf{C}_{2v}''$. Note that each edge coincides with itself (*i.e.* is fixed) by the symmetry operations of $\mathbf{C}_{2v}''$ (or, precisely speaking, one of its conjugate subgroups). The number of edges (12) is equal to the calculated value according to $|\mathbf{O}_h|/|\mathbf{C}_{2v}''| = 48/4 = 12$, where the symbols $|\mathbf{O}_h|$ and $|\mathbf{C}_{2v}''|$ represent the orders of respective point groups. It should be noted here that another CR $\mathbf{O}_h(/\mathbf{C}_{4v})$ has been considered to treat vertex configurations on a regular octahedron [26], whereas the CR $\mathbf{O}_h(/\mathbf{C}_{2v}'')$ should be examined for the present purpose of discussing edge configurations.

Let us consider an edge configuration II, which is obtained by placing four thick edges on the OC–6 (I), as shown in Figure 1. The resulting configuration (II) belongs to $\mathbf{C}_{2h}'$. In the configuration (II), the four occupied edges (thick lines) are equivalent within the operation of $\mathbf{C}_{2h}'$ ($= \{I, C_{2(1)}',$ $\sigma_{d(6)}, i\}$). In addition, the remaining edges can be classified by their superposabilities: the four vacant edges (unmarked), the two vacant edges marked with an open circle ($\circ$), and the two vacant edges marked with a heavy circle ($\bullet$).

The division of edges during the desymmetrization process can be explained by the subduction of a CR. The four occupied edges (thick lines) in II form a four–membered $\mathbf{C}_{2h}'(/\mathbf{C}_1)$–orbit, where $|\mathbf{C}_{2h}'|/|\mathbf{C}_1| = 4/1 = 4$. The symbol $\mathbf{C}_{2h}'(/\mathbf{C}_1)$ corresponds to the fact that the global symmetry of II is $\mathbf{C}_{2h}'$ and the local symmetry of each occupied edge is $\mathbf{C}_1$. The four vacant edges (unmarked) form another four–membered $\mathbf{C}_{2h}'(/\mathbf{C}_1)$–orbit. The two vacant edges marked with an open circle ($\circ$) form a two–membered $\mathbf{C}_{2h}'(/\mathbf{C}_2)$–obit, where $|\mathbf{C}_{2h}'|/|\mathbf{C}_2| = 4/2 = 2$. Finally, the two vacant edges marked with a heavy circle ($\bullet$) form a two–membered $\mathbf{C}_{2h}'(/\mathbf{C}_s)$–orbit, where $|\mathbf{C}_{2h}'|/|\mathbf{C}_s| = 4/2 = 2$. The total process from $\mathbf{O}_h$ to $\mathbf{C}_{2h}'$ is represented by the following subduction of the CR:

$$\mathbf{O}_h(/\mathbf{C}_{2v}'') \downarrow \mathbf{C}_{2h}' = 2\mathbf{C}_{2h}'(/\mathbf{C}_1) + \mathbf{C}_{2h}'(/\mathbf{C}_2) + \mathbf{C}_{2h}'(/\mathbf{C}_s) \tag{1}$$

This subduction is identical with the result shown in the corresponding row of Table 1 that is calculated algebraically by using mark tables [18]. Table 1 also lists the subductions of other subgroups of $\mathbf{O}_h$. Each subduction collected in Table 1 represents an edge partition to produce an edge configuration, where each coset representation (CR) corresponds to an orbit of edges. It can be characterized by its sphericity (enantiospheric, homospheric, and hemispheric) [18,16], if each edge has an inner structure. The sphericity is concisely represented by a dummy variable (*i.e.*, a_d for a homospheric orbit, b_d for a hemispheric orbit, or c_d for an enantiospheric orbit), where the subscript d represents the size of the orbit at issue. Hence, the subduction, which is a sum of CRs, is characterized by means of a product of such dummy variables. The product of dummy variables is called a unit subduced cycle index with chirality fittingness (USCI–CF), which is also listed in Table 1 [16,18].

Table 1. Subduction of $O_h(/C_{2v}'')$

Subgroup $\downarrow G_i$	Subduction $O_h(/C_{2v}'') \downarrow G_i$	USCI–CF	Coefficient
C_1	$12C_1(/C_1)$	b_1^{12}	1/48
C_2	$6C_2(/C_1)$	b_2^6	1/16
C_2'	$5C_2'(/C_1) + 2C_2'(/C_2)$	$b_1^2 b_2^5$	1/8
C_s	$4C_s(/C_1) + 4C_s(/C_s)$	$a_1^4 c_2^4$	1/16
C_s'	$5C_s'(/C_1) + 2C_s(/C_s)$	$a_1^2 c_2^5$	1/8
C_i	$6C_i(/C_1)$	c_2^6	1/48
C_3	$4C_3(/C_1)$	b_3^4	1/6
C_4	$3C_4(/C_1)$	b_4^3	1/8
S_4	$3S_4(/C_1)$	c_4^3	1/8
D_2	$3D_2(/C_1)$	b_4^3	0
D_2'	$2D_2'(/C_1) + D_2'(/C_2) + D_2(/C_2')$	$b_2^2 b_4^2$	0
C_{2v}	$C_{2v}(/C_1) + 2C_{2v}(/C_s) + 2C_{2v}(/C_s')$	$a_2^4 c_4$	0
C_{2v}'	$2C_{2v}'(/C_1) + C_{2v}'(/C_s) + C_{2v}'(/C_s')$	$a_2^2 c_4^2$	0
C_{2v}''	$2C_{2v}''(/C_1) + C_{2v}''(/C_s) + 2C_{2v}''(/C_{2v})$	$a_1^2 a_2 c_4^2$	0
C_{2h}	$2C_{2h}(/C_1) + 2C_{2h}(/C_s)$	$a_2 c_4^2$	0
C_{2h}'	$2C_{2h}'(/C_1) + C_{2h}'(/C_2) + C_{2h}'(/C_s)$	$a_2 c_2 c_4^2$	0
D_3	$D_3(/C_1) + 2D_3(/C_2)$	$b_3^2 b_6$	0
C_{3v}	$C_{3v}(/C_1) + 2C_{3v}(/C_s)$	$a_3^2 c_6$	0
C_{3i}	$2C_{3i}(/C_1)$	c_6^2	1/6
D_4	$D_4(/C_1) + D_4(/C_2'')$	$b_4 b_8$	0
C_{4v}	$2C_{4v}(/C_s) + C_{4v}(/C_s')$	a_4^3	0
C_{4h}	$C_{4h}(/C_1) + C_{4h}(/C_s)$	$a_4 c_8$	0
D_{2d}	$D_{2d}(/C_1) + D_{2d}(/C_s)$	$a_4 c_8$	0
D_{2d}'	$D_{2d}'(/C_2) + 2D_{2d}'(/C_s)$	$a_4^2 c_4$	0
D_{2h}	$D_{2h}(/C_s) + D_{2h}(/C_s') + D_{2h}(/C_s'')$	a_4^3	0
D_{2h}'	$D_{2h}'(/C_1) + D_{2h}'(/C_{2v}) + D_{2h}'(/C_{2v}')$	$a_2^2 c_8$	0
T	$T(/C_1)$	b_{12}	0
D_{3d}	$D_{3d}(/C_2) + D_{3d}(/C_s)$	$a_6 c_6$	0
D_{4h}	$D_{4h}(/C_s) + D_{4h}(/C_{2v})$	$a_4 a_8$	0
O	$O(/C_2')$	b_{12}	0
T_h	$T_h(/C_s)$	a_{12}	0
T_d	$T_d(/C_s)$	a_{12}	0
O_h	$O_h(/C_{2v}'')$	a_{12}	0

The "Coefficient" column of Table 1 shows the sum that is calculated for each subgroup by adding all the values appearing in the corresponding row of the inverse mark table reported previously [26]. In general, the sum of a subgroup is non–zero if it is a cyclic subgroup; otherwise, the sum vanishes. The total of the sums for all the subgroups is equal to 1 [18]. The present enumeration of edge configurations ignore the sphericities so as to substitute a dummy variable s_d for a_d, b_d, and c_d. Thereby, a unit subduced cycle index (USCI) without chirality fittingness is obtained. Among the four methods of the USCI approach that we have proposed for combinatorial enumeration [29,30], we here use the PCI method (the generating–function method based on partial cycle indices (PCIs)) [31]. The USCIs obtained from UCSI–CFs listed in Table 1 are aligned and regarded as a hypothetical row vector. The resulting row vector is multiplied by the inverse mark table (M^{-1}) for O_h [26], where the treatment can be symbolically represented by the expression:

$$(s_1^{12}, s_2^6, s_1^2 s_2^5, s_1^4 s_2^4, s_1^2 s_2^5, \ldots, s_{12}, s_{12}) \times M^{-1}. \tag{2}$$

Thereby, we obtain the partial cycle index (PCI) for every subgroup (Eqs. (3) to (24)), as shown in Table 2 [32].

Table 2. PCIs for Edge Configurations of Octahedral Complexes.

$\text{PCI}(C_1) =$	$(1/48)s_1^{12} - (1/16)s_1^4 s_2^4 - (1/4)s_1^2 s_2^5 - (1/12)s_2^6 - (1/12)s_3^4 + (1/8)s_2^4 s_4 + (1/4)s_1^2 s_2 s_4^2 +$	(3)
	$(5/8)s_2^2 s_4^2 + (1/2)s_3^2 s_6 - (1/8)s_4^3 - (1/2)s_2^2 s_8 - (5/12)s_6^2$	
$\text{PCI}(C_2) =$	$(1/8)s_2^6 - (1/8)s_2^4 s_4 - (3/8)s_2^2 s_4^2 + (3/8)s_4^3 + (1/4)s_2^2 s_8 - (1/4)\,s_4 s_8$	(4)
$\text{PCI}(C_2{'}) =$	$(1/4)s_1^2 s_2^5 - (1/4)s_1^2 s_2 s_4^2 - (1/2)s_2^2 s_4^2 - (1/2)s_3^2 s_6 + (1/2)s_2^2 s_8 + (1/2)s_6^2$	(5)
$\text{PCI}(C_S) =$	$(1/8)s_1^4 s_2^4 - (1/4)s_2^4 s_4 - (1/4)\,s_1^2 s_2 s_4^2 - (1/8)s_2^2 s_4^2 + (1/4)s_4^3 + (1/4)\,s_2^2 s_8$	(6)
$\text{PCI}(C_S{'}) =$	$(1/4)s_1^2 s_2^5 - (1/4)s_1^2 s_2 s_4^2 - (1/2)s_2^2 s_4^2 - (1/2)s_3^2 s_6 + (1/2)s_2^2 s_8 + (1/2)s_6^2$	(7)
$\text{PCI}(C_i) =$	$(1/24)s_2^6 - (3/8)s_2^2 s_4^2 + (1/12)s_4^3 + (1/4)s_2^2 s_8 + (1/3)s_6^2 - (1/3)s_{12}$	(8)
$\text{PCI}(C_3) =$	$(1/4)s_3^4 - (1/2)s_3^2 s_6 + (1/4)s_6^2$	(9)
$\text{PCI}(D_2{'}) =$	$(1/4)s_2^2 s_4^2 - (1/4)s_4^3 - (1/4)\,s_2^2 s_8 + (1/4)s_4 s_8$	(10)
$\text{PCI}(C_{2v}) =$	$(1/4)s_2^4 s_4 - (3/4)s_4^3 + (1/2)s_4 s_8$	(11)
$\text{PCI}(C_{2v}{'}) =$	$(1/4)s_2^2 s_4^2 - (1/4)s_4^3 - (1/4)\,s_2^2 s_8 + (1/4)s_4 s_8$	(12)
$\text{PCI}(C_{2v}{''}) =$	$(1/2)s_1^2 s_2 s_4^2 - (1/2)s_2^2 s_8$	(13)
$\text{PCI}(C_{2h}) =$	$(1/4)s_2^2 s_4^2 - (1/4)s_4^3 - (1/4)\,s_2^2 s_8 + (1/4)s_4 s_8$	(14)
$\text{PCI}(C_{2h}{'}) =$	$(1/2)s_2^2 s_4^2 - (1/2)\,s_2^2 s_8 - s_6^2 + s_{12}$	(15)
$\text{PCI}(D_3) =$	$(1/2)s_3^2 s_6 - (1/2)s_6^2$	(16)
$\text{PCI}(C_{3v}) =$	$(1/2)s_3^2 s_6 - (1/2)s_6^2$	(17)
$\text{PCI}(C_{4v}) =$	$(1/2)\,s_4^3 - (1/2)s_4 s_8$	(18)
$\text{PCI}(D_{2d}{'}) =$	$(1/2)\,s_4^3 - (1/2)s_4 s_8$	(19)
$\text{PCI}(D_{2h}{'}) =$	$(1/6)s_4^3 - (1/2)s_4 s_8 + (1/3)s_{12}$	(20)
$\text{PCI}(D_{2h}{'}) =$	$(1/2)s_2^2 s_8 - (1/2)\,s_4 s_8$	(21)
$\text{PCI}(D_{3d}) =$	$s_6^2 - s_{12}$	(22)
$\text{PCI}(D_{4h}) =$	$s_4 s_8 - s_{12}$	(23)
$\text{PCI}(O_h) =$	s_{12}	(24)

It should be noted that the PCIs for the subgroups C_4, S_4, D_2, C_{3i}, D_4, C_{4h}, D_{2d}, **T**, **O**, T_h, and T_d vanish. This means that edge configurations of these subgroups do not appear in the present enumeration. Strictly speaking, subduced cycle indices (SCIs) should be used in place of USCIs. However, the SCIs are equal to the USCIs in the present enumeration concerning one orbit.

Suppose that a given number (d) of occupied edges (thick edges) are placed on the twelve edges of the octahedral skeleton (I). Then, the dummy variable is substituted by the following edge inventory:

$$s_d = 1 + x^d \qquad (25)$$

which are introduced into the PCIs (eqs. 3 to 24). The resulting equations are expanded to give generating functions for respective subgroups, where the coefficient of the term x^m for each subgroup represents the number of edge configurations with m occupied edges. For example, the introduction of the inventory Eq. (25) into Eq. (3) yields the generating function for the C_1–symmetry as follows:

$$
\begin{aligned}
f_{C1} = &\ (1/48)(1 + x)^{12} - (1/16)(1 + x)^4(1 + x^2)^4 - (1/4)(1 + x)^2(1 + x^2)^5 - (1/12)(1 + x^2)^6 - \\
&\ (1/12)(1 + x^3)^4 + (1/8)(1 + x^2)^4(1 + x^4) + (1/4)(1 + x)^2(1 + x^2)(1 + x^4)^2 \\
&\ + (5/8)(1 + x^2)^2(1 + x^4)^2 + (1/2)(1 + x^3)^2(1 + x^6) - (1/8)(1 + x^4)^3 \qquad (26) \\
&\ - (1/2)(1 + x^2)^2(1 + x^8) - (5/12)(1 + x^6)^2 \\
&\ = 2x^3 + 6x^4 + 10x^5 + 14x^6 + 10x^7 + 6x^8 + 2x^9
\end{aligned}
$$

These coefficients are collected in the **C**$_1$–row of Table 3. The results of all the subsymmetries of **O**$_h$ are listed in Table 3, where the numbers of edge configurations are itemized with respect to point–group symmetries and as well as to the *m* values.

Table 3. Numbers of Edge Configurations [a,b]

	Number of edge configuraions For *m* =													
Symmetry	0	1	2	3	4	5	6	7	8	9	10	11	12	Sum
C$_1$	0	0	0	2	6	10	14	10	6	2	0	0	0	50
C$_2$	0	0	0	0	1	0	0	0	1	0	0	0	0	2
C$_2$'	0	0	1	1	2	4	2	4	2	1	1	0	0	18
C$_s$	0	0	0	2	2	4	2	4	2	2	0	0	0	18
C$_s$'	0	0	1	1	2	4	2	4	2	1	1	0	0	18
C$_i$	0	0	0	0	0	0	0	0	0	0	0	0	0	0
C$_3$	0	0	0	0	0	0	1	0	0	0	0	0	0	1
D$_2$'	0	0	0	0	0	0	1	0	0	0	0	0	0	1
C$_{2v}$	0	0	1	0	0	0	2	0	0	0	1	0	0	4
C$_{2v}$'	0	0	0	0	0	0	1	0	0	0	0	0	0	1
C$_{2v}$"	0	1	0	1	1	2	2	2	1	1	0	1	0	12
C$_{2h}$	0	0	0	0	0	0	1	0	0	0	0	0	0	1
C$_{2h}$'	0	0	0	0	1	0	0	0	1	0	0	0	0	2
D$_3$	0	0	0	1	0	0	0	0	0	1	0	0	0	2
C$_{3v}$	0	0	0	1	0	0	0	0	0	1	0	0	0	2
C$_{4v}$	0	0	0	0	1	0	0	0	1	0	0	0	0	2
D$_{2d}$'	0	0	0	0	1	0	0	0	1	0	0	0	0	2
D$_{2h}$	0	0	0	0	0	0	0	0	0	0	0	0	0	0
D$_{2h}$'	0	0	1	0	0	0	0	0	0	0	1	0	0	2
D$_{3d}$	0	0	0	0	0	0	2	0	0	0	0	0	0	2
D$_{4h}$	0	0	0	0	1	0	0	0	1	0	0	0	0	2
O$_h$	1	0	0	0	0	0	0	0	0	0	0	0	1	2
Sum [c]	1	1	4	9	18	24	30	24	18	9	4	1	1	144

[a] The rows for the subgroup **C**$_4$, **S**$_4$, **D**$_2$, **C**$_{3i}$, **D**$_4$, **C**$_{4h}$, **D**$_{2d}$, **T**, **O**, **T**$_h$, and **T**$_d$ are omitted, because the corresponding PCIs vanish

[b] For a chiral subgroup, an appropriate enantiomer is counted as a representative. In other words, a pair of enantiomers is counted once

[c] It should be noted that Pólya's theorem is merely capable of giving the total vaules contained in this row

The sum of each column is calculated and shown at the bottom row of Table 3. Each value can be calculated alternatively by using the values collected in the "Coefficient" column of Table 1 and the USCIs derived from the USCI–CFs of the same table [18]. Thus, we can obtain the following cycle index (CI):

$$
\begin{aligned}
\mathrm{CI}(s_d) &= (1/48)s_1^{12} + (1/16)s_2^6 + (1/8)\,s_1^2 s_2^5 + (1/16)s_1^4 s_2^4 + (1/8)s_1^2 s_2^5 + (1/48)s_2^6 \\
&\quad + (1/6)s_3^4 + (1/8)s_4^3 + (1/8)s_4^3 + (1/6)s_6^2 \\
&= (1/48)s_1^{12} + (1/16)s_1^4 s_2^4 + (1/4)s_1^2 s_2^5 + (1/12)s_2^6 + (1/6)s_3^4 + (1/4)s_4^3 + (1/6)s_6^2
\end{aligned}
\tag{27}
$$

The resulting CI is generally proved to be equivalent to Pólya's CI [3,4], although the two methods of calculating CIs take quite different procedures [18]. The edge inventory, Eq. (25), is introduced into the CI, Eq. (27), to give the following generating function:

$CI(s_d=1+x^d)$

$$= (1/48)(1+x)^{12} + (1/16)(1+x)^4(1+x^2)^4 + (1/8)(1+x)^2(1+x^2)^5 + (1/12)(1+x^2)^6$$

$$+ (1/6)(1+x^3)^4 + (1/4)(1+x^4)^3 + (1/6)(1+x^6)^2$$

$$= 1 + x + 4x^2 + 9x^3 + 18x^4 + 24x^5 + 30x^6 + 24x^7 + 18x^8 + 9x^9 + 4x^{10} + x^{11} + x^{12}$$

(28)

The coefficients of the terms x^m are identical with the values collected at the bottom row of Table 3. These values validate the previous results obtained manually (or by computer) by Brorson *et al*. [1]. On the other hand, the sum of each row of Table 3 represents the total number of edge configurations for each subgroup. This value can be obtained alternatively by placing $x = 1$ in the edge inventory, Eq. (25), and accordingly by placing $s_d = 1 + 1^d = 2$ in each of the PCIs, *i.e.* Eqs. (3)–(24). Although the PCIs for $\mathbf{C}_i$ and $\mathbf{D}_{2h}$, Eqs. (8) and (20), do not vanish, the present enumeration of edge configurations gives zero values for these symmetries, as confirmed in the following calculations:

$$CI(\mathbf{C}_i; s_d = 2) = \frac{1}{24} \times 2^6 - \frac{3}{8} \times 2^4 + \frac{1}{12} \times 2^3 + \frac{1}{4} \times 2^3 + \frac{1}{3} \times 2^2 - \frac{1}{3} \times 2$$

$$= \frac{1}{3} \times (8 - 18 + 2 + 6 + 4 - 2) = 0$$

(29)

$$CI(\mathbf{D}_{2h}; s_d=2) = \frac{1}{6} \times 2^3 - \frac{1}{2} \times 2^2 + \frac{1}{3} \times 2 = \frac{1}{3} \times (4 - 6 + 2) = 0$$

(30)

As found easily by the inspection of Table 3, the number of edge configurations for m is equal to the counterpart for $12 - m$ for each row (point–group symmetry). This means that the concept of the complementary configuration introduced by Brorson *et al*. [1] can be elaborated to take account of symmetries as discussed below.

3 CHIRAL EDGE CONFIGURATIONS

The edge configurations listed in the $\mathbf{C}_1$–row of Table 3 are depicted in Figure 2, where an arbitrary enantiomer is depicted as a representative for a pair of enantiomers. Since an edge configuration with m occupied edge always corresponds to the counterpart (complementary configuration) with $12 - m$ occupied edges (within $m < 6$), Figure 2 (also the other figures) contains the edge configurations of $m < 6$ along with those of $m = 6$ for the sake of simplicity. Thus, 32 edge configurations are selected from the 50 edge configurations enumerated in the $\mathbf{C}_1$–row of Table 3.

Since the subduction table (Table 1) indicates the partition of edges for each symmetry, it is easy to depict each edge configuration belonging to the symmetry. For example, a $\mathbf{C}_2$–edge configuration has six two–membered $\mathbf{C}_2(/\mathbf{C}_1)$–orbits, as shown in the $\mathbf{C}_2$–row of Table 1. The resulting edge configuration can be depicted as **33** in Figure 3, where the relevant two–fold axis runs through the top and bottom vertices. There is only one edge configuration of $m = 4$ under the condition of $m \le 6$

in accord with the enumeration result shown in Table 3. On the other hand, C_2'–edge configurations are based on the two–fold axis intersecting the front and back edges, as found in the edge configurations **34** to **43**. Note that all the packing modes of occupied edges (thick edges) and unoccupied edges (thin edges) are in agreement with the subduction listed in the C_2'–row of Table 1. These edge configurations are classified in terms of the enumeration results shown in Table 3.
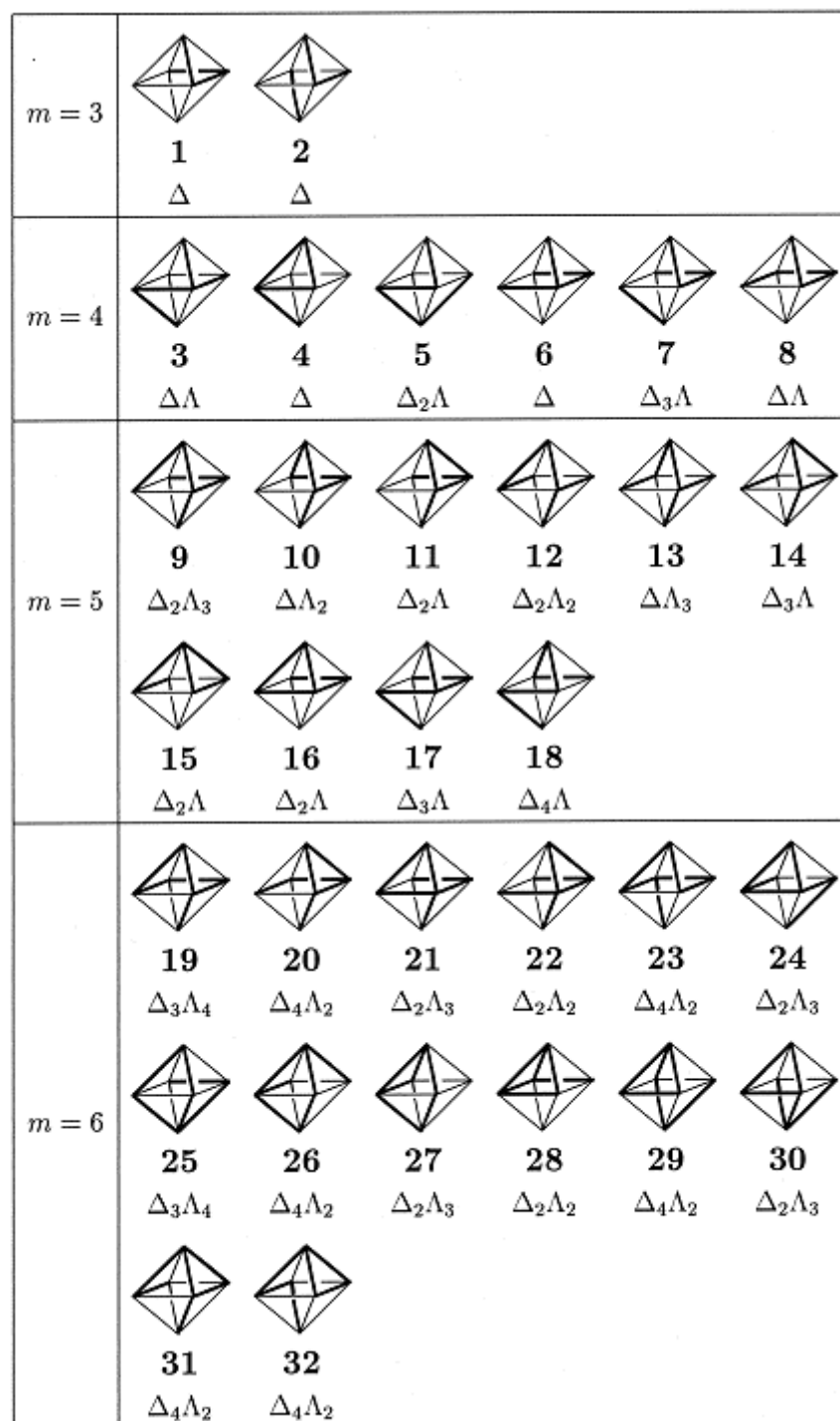
Figure 2. Asymmetric edge configurations (C_1–symmetry for $m \leq 6$).

Figure 3. Chiral edge configurations other than asymmetric ones ($m \leq 6$).

4 ACHIRAL EDGE CONFIGURATIONS

Figure 4 depicts edge configurations of $\mathbf{C}_s$– and $\mathbf{C}_s$'–symmetries ($m \leq 6$). As found in the $\mathbf{C}_s$–edge configurations **47** to **56**, the mirror plane for the $\mathbf{C}_s$–symmetry is selected here as the horizontal plane that is perpendicular to the two–fold axis through the top and bottom vertices. All the packing modes of occupied edges (thick edges) and unoccupied edges (thin edges) in **47** to **56** are in agreement with the subduction listed in the $\mathbf{C}_s$–row of Table 1. The numbers of the depicted

edge configurations are in agreement with the enumeration results shown in the C_s–row of Table 3. The edge configurations **57** to **66** belong to the C_s'–symmetry ($m \leq 6$), where the itemization with respect to the m values is in agreement with the enumeration results shown in the C_s'–row of Table 3. The mirror plane selected for **57** to **66** is the plane that contains the top and bottom vertices and bisects the front and back edges. The packing mode of occupied and unoccupied edges in each of the edge configurations **47** to **56** is in agreement with the subduction listed in the C_s'–row of Table 1.

Figure 4. Edge configurations of C_s– and C_s'–symmetries ($m \leq 6$).

Figure 5 depicts edge configurations of C_{2v}–like and C_{2h}–like subsymmetries ($m \leq 6$). The C_{2v}–, C_{2v}'– and C_{2h}–symmetries have the common two–fold axis with C_2, while the C_{2v}"– and C_{2h}'–symmetries are based on the two–fold axis of C_2'. The packing modes in these edge configurations are in agreement with the corresponding rows of Table 1. The numbers of the depicted edge configurations are in agreement with the enumeration results shown in the corresponding rows of Table 3.

Figure 6 depicts achiral edge configurations having a three–fold axis ($m \leq 6$). The packing modes in these edge configurations are in agreement with the corresponding rows of Table 1. The numbers of the depicted edge configurations are in agreement with the enumeration results shown in the corresponding rows of Table 3.

	$m = 1$	$m = 2$	$m = 3$	$m = 4$	$m = 5$	$m = 6$
C_{2v}		67				68 69
C_{2v}'						70
C_{2v}''	71		72	73	74 75	76 77
C_{2h}						78
C_{2h}'				79		

Figure 5. Edge configurations of C_{2v}–, C_{2v}'–, C_{2v}''–, C_{2h}–, and C_{2h}'–symmetries ($m \leq 6$)

Figure 7 depicts remaining achiral edge configurations ($m \leq 6$), where the edge configuration with no occupied edges (O_h) is omitted. The packing modes in these edge configurations are in agreement with the corresponding rows of Table 1. The numbers of the depicted edge configurations are in agreement with the enumeration results shown in the corresponding rows of Table 3.

	$m = 2$	$m = 3$	$m = 4$	$m = 5$	$m = 6$
C_{3v}		**80**			
D_{3d}					**81** **82**

Figure 6. Edge configurations of C_{3v}– and D_{3d}–symmetries ($m \leq 6$).

	$m = 2$	$m = 3$	$m = 4$	$m = 5$	$m = 6$
C_{4v}			**83**		
D'_{2d}			**84**		
D'_{2h}	**85**				
D_{4h}			**86**		

Figure 7. Edge configurations of C_{4v}–, D_{2d}'–, D_{2h}'–, and D_{4h}–symmetries ($m \leq 6$).

5 COMPLEMENTARY EDGE CONFIGURATIONS

The complementary configuration of a given configuration with m occupied edges has been defined as the configuration made up by the remaining $12 - m$ edges [1]. It is also known that, if a

chiral edge configuration has the chiral descriptor $\Delta_\delta \Lambda_\lambda$, its complementary configuration has $\Delta_{\delta+12-2m} \Lambda_{\lambda+12-2m}$, as proved by Brorson *et al*. [1]. This section is devoted to give an alternative proof of this relationship and further aspects of complementary configurations.

5.1 Chiral Descriptors for Complementary Configurations

Suppose that a chiral edge configuration with *m* occupied edges has the chiral descriptor $\Delta_\delta \Lambda_\lambda$ and that the occupied edges are numbered with the numbers $k = 1, 2, \ldots, m$. To an extreme case, the edge with the number *k* may have two Δ−edges and two Λ−edges to be determined for the chiral descriptor. If an edge selected from the two Δ edges contributes the Δ_δ part of the descriptor $\Delta_\delta \Lambda_\lambda$, the pair of the edge *k* and the selected edge is called an "effective edge pair" for the sake of simplicity. Otherwise, it is called an "ineffective edge pair", since it is ineffective to the chiral descriptor. Note that the edge *k* and the two Δ−edges (effective or ineffective) are placed in the same relationship as the three thick lines of **46** shown in Figure 3. Let δ_k and $\delta_k{}'$ be the numbers of effective and ineffective edge pairs, respectively, with respect to the edge *k*. Then, we can place $\delta_k + \delta_k{}' = 2$. When *k* runs from 1 to *m*, we can place $\sum_{k=1}^m \delta_k + \sum_{k=1}^m \delta_k{}' = 2m$. Obviously, we have $2\delta = \sum_{k=1}^m \delta_k$ for the total number of effective edge pairs, since each effective edge pair is counted twice. On the other hand, we have $\delta' = \sum_{k=1}^m \delta_k{}'$ for the total number of ineffective edges. Hence, we obtain $2\delta + \delta' = 2m$. The same discussion can be applied to the corresponding complementary configuration having the chiral descriptor $\Delta_{\tilde\delta} \Lambda_{\tilde\lambda}$. Thereby, we can obtain $2\tilde\delta + \delta' = 2(12 - m)$, where the number of ineffective edge pairs (δ') is common according to the complementary relationship. By deleting δ' from the two equations, we arrive at $\tilde\delta = \delta + 12 - 2m$. The same discussion is available for the Λ−parts of the complementary chiral descriptors ($\Delta_\delta \Lambda_\lambda$ and $\Delta_{\tilde\delta} \Lambda_{\tilde\lambda}$) to give $\tilde\lambda = \lambda + 12 - 2m$. It follows that the chiral descriptor $\Delta_\delta \Lambda_\lambda$ is complementary to $\Delta_{\delta+12-2m} \Lambda_{\lambda+12-2m}$.

5.2 Paired Complementary Configurations

Each edge configuration with $m \leq 5$ has its complementary configuration belonging to the same point group as the original one. Edge configurations with $m = 6$ behave differently. Each edge configuration in the first row of $m = 6$ in Figure 2 is complementary to the counterpart in the second row of $m = 6$. Since $12 - 2m = 0$ for $m = 6$, the chiral descriptor $\Delta_\delta \Lambda_\lambda$ is identical with the complementary one $\Delta_{\delta+12-2m} \Lambda_{\lambda+12-2m}$. For example, the edge configuration **19** and the corresponding complementary one **25** have the same chiral descriptor $\Delta_3 \Lambda_4$. The edge configuration **42** is complementary to the enantiomer of **43**, as shown in Figure 3.

As for achiral edge configurations, there also appear complementary relationships for $m = 6$, *e.g.*, the $\mathbf{C}_s{}'$ pair of **65** and **66** in Figure 4, the $\mathbf{C}_{2v}$ pair of **68** and **69** in Figure 5, the $\mathbf{C}_s{}''$ pair of **76** and **77** in Figure 5, and the $\mathbf{D}_{3d}$ pair of **81** and **82** in Figure 6.

5.3 Self–Complementary Configurations

The edge configuration **31** is self–complementary so that **31** is homomeric to the corresponding complementary configuration. This phenomenon is ascribed to the presence of the subduction $6C_2(/C_1)$, which involves the subduction $12C_1(/C_1)$ (for **31**) in a homomeric fashion. In other words, the partition of the twelve edges of a regular octahedron into the set of the edges for **31** and the set of the remaining ones (i.e. the edges for its complementary configuration) produces a C_2–object of the two sets. The two sets form a hemispheric orbit ascribed to $C_2(/C_1)$, where the local symmetry C_1 is the symmetry of the edge configuration **31**. The self–complementary behavior of the edge configuration **32** can be similarly explained.

The edge configuration **44** is a special case of self–complementary relationships, so that **44** is enantiomeric to the corresponding complementary configuration. This is ascribed to the presence of the subduction $2C_{3i}(/C_1)$, which involves the subduction $4C_3(/C_1)$ in an enantiomeric fashion. In other words, the partition of the twelve edges of a regular octahedron into the set of the edges for **44** and the set of the edges for its complementary configuration produces a C_{3i}–object of the two sets. The two sets form an enantiospheric orbit that is ascribed to $2C_{3i}(/C_3)$, where the local symmetry C_3 is the symmetry of the edge configuration **44**.

The edge configuration **45** is self–complementary, where **45** is homomeric to the corresponding complementary configuration. This is ascribed to the presence of the subduction $D_4(/C_1) + D_4(/C_2'')$, which involves the subduction $2D_2'(/C_1) + D_2'(/C_2) + D_2'(/C_2')$ in a homomeric fashion. The partition of the twelve edges of a regular octahedron into the set of the edges for **45** and the set of the edges for its complementary configuration produces a D_4–object of the two sets. The two sets form a hemispheric orbit that is ascribed to $D_4(/D_2')$, where the local symmetry D_2' is the symmetry of the edge configuration **45**.

Self–complementary relationships are also observed for achiral edge configurations. For example, the C_s–configurations **55** and **56** in Figure 4 are self–complementary respectively. This is ascribed to the presence of the subduction $2C_{2v}'(/C_1) + C_{2v}'(/C_s) + C_{2v}'(/C_s')$, which involves the subduction $4C_s(/C_1) + 4C_s(/C_s)$ in a homomeric fashion. The set of the edges for **55** (or **56**) and the set of the edges for its complementary configuration form a C_{2v}'–object. The two sets form a homospheric orbit that is ascribed to the CR $C_{2v}'(/C_s)$, where the local symmetry C_s is the symmetry of the edge configuration **55** (or **56**).

The C_{2v}'–configuration **70** in Figure 5 is self–complementary. This is ascribed to the presence of the subduction $D_{4h}(/C_s) + D_{4h}(/C_{2v})$, which involves the subduction $2C_{2v}'(/C_1) + C_{2v}'(/C_s) + C_{2v}'(/C_s')$ in a homomeric fashion. This case can be similarly explained by $D_{4h}(/C_{2v}')$, where the local symmetry C_{2v}' is the symmetry of the edge configuration **70**.

The C_{2h}–configuration **78** in Figure 5 is self–complementary. This is ascribed to the presence of the subduction $D_{4h}(/C_s) + D_{4h}(/C_{2v})$, which involves the subduction $2C_{2h}(/C_1) + 2C_{2h}(/C_s)$ in a

homomeric fashion. This case can be explained by $\mathbf{D}_{4h}(/\mathbf{C}_{2h})$, where the local symmetry $\mathbf{C}_{2h}$ is the symmetry of the edge configuration **78**.

The discussion described above can be extended to a more general case in which the edges of a **G**–object (*e.g.*, $\mathbf{O}_h$) are divided into two parts so as to give a $\mathbf{G}_i$–object with the two parts. If the two parts form two distinct orbits that are ascribed to $2\mathbf{G}_i(/\mathbf{G}_i)$, they correspond to a pair of complementary configurations. The local symmetry $\mathbf{G}_i$ is the same as those of the complementary configurations. If the the two pairs form a two–membered orbit that is ascribed to $\mathbf{G}_i'(/\mathbf{G}_i)$, they correspond to a self–complementary configuration, where $\mathbf{G}_i'$ is a supergroup of $\mathbf{G}_i$ ($|\mathbf{G}_i'|/|\mathbf{G}_i| = 2$). The local symmetry $\mathbf{G}_i$ is the same as that of the self–complementary configuration.

6 EDGE CONFIGURATIONS WITH TERDENTATE LIGANDS

Edge configurations with a terdentate ligand correspond to the ones with adjacent occupied edges ($m = 2$). They are **57** of $\mathbf{C}_s'$–symmetry in Figure 4 and **67** of $\mathbf{C}_{2v}$–symmetry in Figure 5. Edge configurations with two terdentate ligands correspond to cases with two sets of adjacent occupied edges ($m = 4$). They are found to be **37** of $\mathbf{C}_2'$–symmetry in Figure 3, **79** of $\mathbf{C}_{2h}'$–symmetry in Figure 5, and **84** of $\mathbf{D}_{2d}'$–symmetry in Figure 7. It should be emphasized here that the USCI approach itemizes the symmetry of each edge configuration, clarifying the non–existence of edge configurations of the $\mathbf{C}_i$–symmetry, see Table 3 and Eq. (30). The edge configuration **79** has once been assigned to such $\mathbf{C}_i$–symmetry in von Zelewsky's textbook (No. 31 described on p. 119 in Ref. [2]).

Although **84** of $\mathbf{D}_{2d}'$–symmetry (Figure 7) is achiral as the edge configuration, the non–planarity of the central atom may change **84** into a chiral configuration, as discussed in pages 119–121 of von Zelewsky's textbook. This desymmetrization is more elaborately explained in terms of the concept of mismatched molecules [33]. In **84**, the orbit of the vertices accommodating the central atom is ascribed to the CR $\mathbf{D}_{2d}'(/\mathbf{C}_{2v})$, which is produced by the following subduction [26]:

$$\mathbf{O}_h(/\mathbf{C}_{4v})\downarrow \mathbf{D}_{2d}' = 2\mathbf{D}_{2d}'(/\mathbf{C}_s) + \mathbf{D}_{2d}'(/\mathbf{C}_s) + \mathbf{D}_{2d}'(/\mathbf{C}_{2v}) \tag{31}$$

Let us now consider the ligand $H_2NCH_2CH_2$–NH–$CH_2CH_2NH_2$. The non–planarity of the central ligand atom in such a configuration as **84** is determined to be $\mathbf{C}_1$, which is mismatched to the local symmetry $\mathbf{C}_{2v}$. According to this mismatch, the global symmetry is reduced so as to compensate the mismatch. This is accomplished by the following subduction:

$$\mathbf{O}_h(/\mathbf{C}_{4v})\downarrow \mathbf{C}_2' = 3\mathbf{C}_2'(/\mathbf{C}_1) \tag{32}$$

The resulting local symmetry $\mathbf{C}_1$ satisfies the $\mathbf{C}_1$ due to the non–planarity. It follows that the resulting complex belongs to $\mathbf{C}_2'$–symmetry at the highest attainable conformation.

7 CONCLUSIONS

The complete set of octahedral edge configurations is obtained by virtue of the USCI (unit–subduced–cycle–index) approach, where the set is itemized with respect to two criteria, *i.e.*, the numbers of edges and the point–group symmetries. The latter criterion enables us to examine chiral and achiral edge configurations. Complementary configurations are discussed in terms of the subductions of coset representations (CRs). Thus the versatility of the USCI approach is demonstrated in characterizing inorganic complexes.

Acknowledgment

5 REFERENCES

[1]   M. Brorson, T. Damhus, C. E. Schäffer, Exhaustive Examination of Chiral Configurations of Edges on a Regular Octahedron: Analysis of the Possibilities of Assigning Chirality Descriptors within a Generalized Δ/Λ System, *Inorg. Chem.* **1983**, *22*, 1569–1573.

[2]   A. von Zelewsky; *Stereochemistry of Coordination Compounds*. John Wiley & Sons: Chichester, 1996.

[3]   G. Pólya, Tabelle der Isomerenzahlen für die einfacheren Derivate einiger chyclischen Stammkörper, *Helv. Chim. Acta* **1936**, *19*, 22—24.

[4]   G. Pólya, R. C. Read, *Combinatorial Enumeration of Groups*, *Graphs*, *and Chemical Compounds*. Springer–Verlag: New York, 1987.

[5]   B. A. Kennedy, D. A. McQuarrie, C. H. Brubaker, Jr., Group Theory and Isomerism, *Inorg. Chem.* **1964**, *3*, 265–268.

[6]   D. H. McDaniel, A Restatement of Polya's Theorem, *Inorg. Chem.* **1972**, *11*, 2678–2682.

[7]   Pioneering enumerations of inorganic complexes by using Pólya's theorem were reported [5,6]. It should be added here that even the methods of the first generation (e.g., Pólya's theorem) have their own merits. If the chemist who has to find the number of possible isomers of a molecule does not go to the trouble of using them (regarding them as abstruse mathematical methods), the validity of his/her results cannot be assured. Instead, his/her algorithm should be proved correct by using mathematical methods of another abstruse type. However, the latter proof is frequently omitted. This is the reason for using the expressions "he/she believed" and "almost equivalent results" in the text. It should be noted that the methods of the first generation provide the basis of assuring the validity of his/her results.

[8]   J. Sheehan, The Number of Graphs with a Given Automorphism Group, *Canad. J. Math.* **1968**, *20*, 1068—1076.

[9]   A. Kerber, K.–J. Thürlings, Counting Symmetry Classes of Functions by Weight and Automorphism Group, In *Combinatorial Theory*; D. Jngnickel, K. Vedder, Eds.; Springer: Berlin, 1982; pp 191–211.

[10]   W. Hässelbarth, Substitution symmetry, *Theor. Chim. Acta* **1985**, *67*, 339–367.

[11]   J. Brocas, Double Cosets and Enumeration of Permutational Isomers of Fixed Symmetry, *J. Am. Chem. Soc.* **1986**, *108*, 1135–1145.

[12]   C. A. Mead, Table of Marks and Double Cosets in Isomer Counting, *J. Am. Chem. Soc.* **1987**, *109*, 2130–2137.

[13]   E. K. Lloyd, Marks of Permutation Groups and Isomer Enumeration, *J. Math. Chem.* **1992**, *11*, 207–222.

[14]   W. Burnside, *Theory of Groups of Finite Order*, 2nd ed. Cambridge University Press: Cambridge, 1911.

[15]   J. A. Pople, Classification of Molecular Symmetry by Framework Groups, *J. Am. Chem. Soc.* **1980**, *102*, 4615–4622.

[16]   S. Fujita, Chirality Filltingness of an Orbit Governed by a Coset Representation. Integration of Point–group and Permutation–group Theories to Treat Local Chirality and Prochirality, *J. Am. Chem. Soc.* **1990**, *112*, 3390–3397.

[17]   S. Fujita, Systematic Characterization of Prochirality, Prostereogenicity, and Stereogenicity by Means of the Sphericity Concept, *Tetrahedron* **2000**, *56*, 735–740.

[18]   S. Fujita, *Symmetry and Combinatorial Enumeration in Chemistry*. Springer–Verlag: Berlin–Heidelberg, 1991.

[19]   S. Fujita, Stereogenicity Based on Orbits Governed by Coset Representations, *Tetrahedron* **1990**, *46*, 5943–5954.

[20]   S. Fujita, Anisochrony and Symmetry Non–Equivalence Characterized by Subduction of Coset Representations, *Bull. Chem. Soc. Jpn.* **1991**, *64*, 439–449.

[21] S. Fujita, Subduction of Coset Representations. An Application to Enumeration of Chemical Structures, *Theor. Chim. Acta* **1989**, *76*, 247–268.

[22] S. Fujita, Sphericity Governs Both Stereochemistry in a Molecule and Stereoisomerism Among Molecules, *Chem. Rec.* **2002**, *3*, 164–176.

[23] S. Fujita, Sphericity beyond Topicity in Characterizing Stereochemical Phenomena. Novel Concepts Based on Coset Representations and Their Subductions, *Bull. Chem. Soc. Jpn.* **2002**, *75*, 1863–1883.

[24] S. Fujita, Systematic Classification of Molecular Symmetry by Subductions of Coset Representations, *Bull. Chem. Soc. Jpn.* **1990**, *63*, 315–327.

[25] S. Fujita, Subductive and Inductive Derivation for Designing Molecules of High Symmetry, *J. Chem. Inf. Comput. Sci.* **1991**, *31*, 540–546.

[26] S. Fujita, Promolecules with a Subsymmetry of O_h. Combinatorial Enumeration and Stereochemical Properties, *Polyhedron* **1993**, *12*, 95–110.

[27] S. Fujita, Systematic Enumeration of Ferrocene Derivatives by Unit–Subduced–Cycle–Index Method and Characteristic–Monomial Method, *Bull. Chem. Soc. Jpn.* **1999**, *72*, 2409–2416.

[28] G. J. Leigh, *Nomenclature of Inorganic Chemistry*. Blackwell: Oxford, 1990.

[29] S. Fujita, Subduction of Coset Representations. An Application to Enumeration of Chemical Structures with Achiral and Chiral Ligands, *J. Math. Chem.* **1990**, *5*, 121–156.

[30] S. Fujita, Systematic Enumeration of High Symmetry Molecules by Unit Subduced Cycle Indices With and Without Chirality Fittingness, *Bull. Chem. Soc. Jpn.* **1990**, *63*, 203–215.

[31] S. Fujita, Unit Subduced Cycle Indices and the Superposition Theorem. Derivation of a New Theorem and Its Application to Enumeration of Compounds Based on a D_{2d} skeleton, *Bull. Chem. Soc. Jpn.* **1990**, *63*, 2770–2775.

[32] The inverse mark table (Table 2) reported in Ref. [26] contains the following typing errors in the $O_h(/D_2')$–column: The non–zero values 1/4, 1/4, 1/4, 1/4, and 1/2 should be corrected into 1/4, –1/4, –1/4, –1/4, and 1/2.

[33] S. Fujita, Promolecules for Characterizing Stereochemical Relationships in Non–Rigid Molecules, *Tetrahedron* **1991**, *47*, 31–46.

Biographies

Shinsaku Fujita is Professor of Information Materials Technology at Kyoto Institute of Technology (KIT). After obtaining a Dr. Eng. degree at Kyoto University under the guidance of Prof. Hitosi Nozaki, he joined the Research Laboratories of Fuji Photo Film Co., Ltd. in Ashigara, Japan in 1972. In 1982, he was awarded the Synthetic Organic Chemistry Award. Beginning in 1997, he has served as a professor at KIT. His research interests have included reactive intermediates, synthetic organic chemistry, organic photochemistry, organic stereochemistry, mathematical organic chemistry, and organic reaction databases. He is the author of *Symmetry and Combinatorial Enumeration in Chemistry* (Springer–Verlag, 1991), *XyMTeX——Typesetting Chemical Structural Formulas* (Addison–Wesley Japan, 1997), *Computer–Oriented Representation of Organic Reactions* (Yoshioka Shoten, 2001), and several books on TeX/LaTeX. His home page on the World Wide Web is located at http://imt.chem.kit.ac.jp/fujita/fujitas/fujita.html.

Nobukazu Matsubara is a graduate student at Kyoto Institute of Technology.